Divergence in Nonspecific Hydrophobic Packing Interactions in the Apo State, and Its Possible Role in Functional Specialization of Mitochondrial and Microsomal Cytochrome b_5[†]

Aaron B. Cowley, Na Sun, Mario Rivera, and David R. Benson*

Department of Chemistry, University of Kansas, Lawrence, Kansas 66045

Received July 12, 2005; Revised Manuscript Received September 6, 2005

ABSTRACT: The outer mitochondrial membrane isoform of mammalian cytochrome b_5 (OM b_5) is distinguished from the microsomal isoform (Mc b_5) by its considerably greater stability. In contrast, OM and Mc apocytochrome b_5 (apo-b_5) exhibit similar thermodynamic stability. Contributing substantially to the greater stability of OM b_5 relative to that of Mc b_5 is the presence of Leu at position 71. Replacing Leu-71 in OM b_5 with the corresponding Mc b_5 residue (Ser) not only diminishes holoprotein stability but also markedly compromises apoprotein stability. The studies reported herein were undertaken to clarify the role played by Leu-71 in stabilizing OM b_5s relative to Mc b_5s, and were motivated by the possibility that stability is related to other differences in OM and Mc b_5 properties that are important for their specialized subcellular roles. The results of these studies show that Leu-71 plays an essential role in maintaining the structural integrity of the heme-independent folding core of OM apo-b_5 (core 2), despite its location in the disordered empty heme-binding pocket (core 1). The conformational integrity of core 2 in Mc apo-b_5s is not similarly dependent on the presence of a hydrophobic residue at position 71, providing new evidence for evolution of compensating structural features not present in OM b_5s. We propose that Leu-71 achieves its effect on OM apo-b_5 core 2 structure by participating in a nonspecific hydrophobic collapse of disordered core 1, templated by more conformationally restricted side chains of residues in the β-sheet that separates the two cores. We hypothesize that this has the added effect of maintaining core 1 of OM apo-b_5s in a state more compact than that which occurs in Mc apo-b_5s, possibly contributing to stronger heme binding by limiting the number of non-native conformations that the empty heme-binding pocket can populate.

Mammals produce two membrane-anchored isoforms of cytochrome b_5 that are targeted to distinct subcellular locations, one to the endoplasmic reticulum (microsomal, or Mc b_5) and the other to the mitochondrial outer membrane (OM b_5) (*1*, *2*). Each isoform is tail-anchored to the membrane of its respective organelle by a C-terminal hydrophobic domain, with its polar N-terminal heme-binding domain extending into the cytosol (*3*, *4*). Amino acid sequences of recombinant polypeptides representing the heme-binding domains of bovine Mc b_5 (bMc b_5)[1] and rat OM b_5 (rOM b_5), which have been the focus of comparative biophysical studies in our laboratories (*5*−*9*), are aligned in Figure 1. The availability of X-ray crystal structures of bMc (*10*) and rOM b_5 (*11*) prompted their use in our studies, a decision justified by the strong conservation of amino acid sequences of mammalian Mc and OM b_5s across species (*12*). For example, the heme-binding domain of rat Mc (rMc) b_5 differs from that of bMc b_5 at only four positions when considering residues involved in specific packing interactions, with all substitutions conservative and three involving solvent-exposed side chains. Available theoretical (*13*, *14*) and experimental (*12*, *14*, *15*) evidence also suggests strong conservation of structural and biophysical properties among Mc and OM b_5s from different mammals.

```
          -1 1          11          21          31
bMc          AVKYYTLE EIQKHNNSKS TWLILHYKVY DLTKFLEEHP
rOM  NGQGS DPAVTYYRLE EVAKRNTAEE TWMVIHGRVY DITRFLSEHP
                  β1  α1          β4    β3    α2

    41          51          61          71          81
bMc  GGEEVLREQA GGDATENFED VGHSTDAREL SKTFIIGELH PDDR
rOM  GGEEVLLEQA GADATESFED VGHSPDAREM LKQYYIGDVH PNDLKPK
          α3    β5  α4          α5    β2    α6
```

FIGURE 1: Amino acid sequences of the recombinant bMc and rOM b_5 polypeptides used in this study, highlighting the units of secondary structure. Numbering is based on the scheme introduced by Mathews for the 93-residue lipase fragment of bovine Mc b_5 (*41*). The italicized residues at the N- and C-termini of the rOM b_5 sequence are unstructured in the holoprotein crystal structure.

Mc and OM b_5 heme-binding domains exhibit virtually identical three-dimensional folds with $\beta1-\alpha1-\beta4-\beta3-\alpha2-\alpha3-\beta5-\alpha4-\alpha5-\beta2-\alpha6$ topology, comprising two hydrophobic cores. As highlighted in Figure 2A for bMc b_5, core 1 contains a heme surrounded by helices $\alpha2-\alpha5$ while core 2 contains helices $\alpha1$ and $\alpha6$. Strand 5 of the β-sheet

[†] This work was supported by a grant from the National Science Foundation (MCB-0446326).

* To whom correspondence should be addressed. Phone: (785) 864-4090. Fax: (785) 864-5396. E-mail: drb@ku.edu.

[1] Abbreviations: rOM b_5, rat outer mitochondrial membrane cytochrome b_5; bMc b_5, bovine microsomal cytochrome b_5; apo-b_5, apocytochrome b_5; CD, circular dichroism; DLS, dynamic light scattering; DSC, differential scanning calorimetry; GRAVY, grand average of hydropathicity.

10.1021/bi051337m CCC: $30.25
Published on Web 10/14/2005

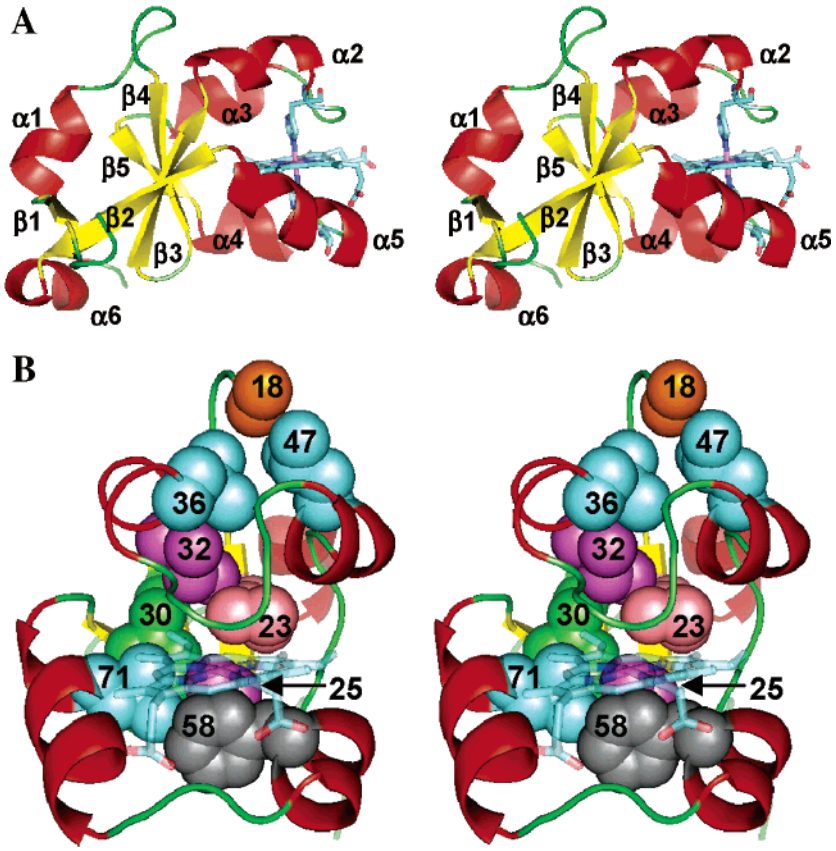

FIGURE 2: (A) Stereo representation of the X-ray crystal structure of bMc b_5 highlighting the elements of secondary structure. (B) Stereoview of the corresponding rOM b_5 structure showing side chains of amino acids contributing to the extended hydrophobic packing interactions described in the text. Amino acid side chains are labeled with the residue number and are color-coded as follows: gray for Phe, green for Tyr, cyan for Leu, magenta for Ile, salmon for Met, and orange for Ala.

separates α3 and α4 and is thus formally part of core 1, but for reasons discussed below, β1−β4 are generally considered to be part of core 2. It is important to emphasize that side chains of amino acids in β2−β4 contribute to tertiary structure in both core 1 and core 2.

Early studies with Mc b_5s showed that the polypeptide retains significant secondary and tertiary structure following dissociation of heme, but that the apoprotein is expanded and destabilized relative to the holoprotein (*16*). Computational studies comparing bMc and rMc apo-b_5 suggested that conformational disruption arising from heme loss is more extensive in core 1 than in core 2 (*13*). Indeed, nuclear magnetic resonance (NMR) studies of rMc apo-b_5 published subsequently revealed that core 1 is conformationally disordered while core 2 retains a holo-like fold (*17*, *18*). Recent studies in our laboratories have indicated that the same situation holds for OM apo-b_5s (*7*). We have also shown that rOM and bMc apo-b_5 exhibit similar thermodynamic stabilities in aqueous solution (unfolding free energies of ~3 kcal/mol at pH 7 and 25 °C) (*7*, *8*). In striking contrast, OM holo-b_5s are significantly more stable than Mc holo-b_5s due to a higher kinetic barrier for heme dissociation (*8*, *12*). For example, OM b_5s do not lose hemin (ferric heme) to apomyoglobin at pH 7 and 37 °C, while the corresponding reactions of Mc b_5s are complete within a couple of days.

Molecular dynamics (MD) simulations (*5*, *19*) and hydrogen−deuterium exchange experiments monitored by NMR spectroscopy (*9*) have provided strong evidence for lower polypeptide dynamic mobility in core 1 of OM b_5s relative to that in Mc b_5s. This suggests that the higher stability exhibited by the OM proteins may be a consequence of less frequent conformational disruptions that can trigger heme dissociation. Another possible contributor, more efficient rebinding of heme following a given dissociation event, was suggested by dynamic light scattering (DLS) data indicating that core 1 is more compact and less conformationally dynamic in rOM apo-b_5 than in bMc apo-b_5 (*7*). We have proposed (*7*, *9*) that the lower holoprotein dynamic mobility and greater apoprotein compactness distinguishing OM b_5s from Mc b_5s are manifestations of greater hydrophobicity in their heme-binding pockets, arising from two conserved packing motifs (A and B) involving the side chains of amino acids in α2−α5 and the core 1 side of the β-sheet (*5*, *6*, *12*). As shown in Figure 2B for rOM b_5, motif A begins at the protein surface with van der Waals contact between the side chains of Ala-18 (in a core 2 surface loop separating α1 and β4) and Leu-47 (in α3 of core 1). The motif extends into the protein interior via successive hydrophobic contacts between (1) the Leu-47 side chain and that of Leu-36, located near the center of core 1 helix α2; and (2) the Leu-36 side chain and the β-CH_3 group of Ile-32, the residue bridging β3 in core 2 and α2 in core 1. Motif B in OM b_5s involves mutual van der Waals contact among heme, the buried side chains of Phe-58 in α4 and Ile-25 in β4, and the partially solvent-exposed side chain of Leu-71 in the last turn of α5. Figure 2B shows two additional interactions extending these motifs whose importance became apparent during the studies reported herein. One is between the side chain of Leu-71 and the aromatic ring of Tyr-30 in β3. The other involves the heme and the side chains of motif A residue Ile-32 and

motif B residues Ile-25 and Met-23 (located two residues away from Ile-25 in β4). Motifs A and B in OM b_5s thus represent segments of a larger hydrophobic network spanning the base of the heme-binding pocket and ending in contact with solvent at both ends. The only known variations in this network, in human OM b_5 (Leu at positions 18 and 23, β-branched Val at position 32), are not expected to affect the fundamental nature of the hydrophobic network (*12*).

Mc b_5s have three residues in common with OM b_5s in the motif A/B region, all of which are highly conserved in the b_5 family: Leu-36, Phe-58, and Tyr-30. Mc b_5s also share with OM b_5s the presence of residues with hydrophobic side chains at positions 23 (Leu or Val), 25 (Leu), and 32 (Leu) that engage in mutual interactions with one another and with heme. Packing in Mc b_5s in the region corresponding to OM b_5 motifs A and B involves a much less extended hydrophobic network, however, with the greatest contribution due to the presence of residues with polar side chains at solvent-exposed positions 18 (Ser), 47 (Arg), and 71 (Ser). In the bMc b_5 crystal structure, the Ser-18 and Arg-47 side chains appear to make a polar contact on the protein surface, and the Arg-47 side chain makes hydrophobic contact with that of Leu-36. In contrast to the Ala-18−Leu-47 hydrophobic contact in rOM b_5, however, the Ser-18−Arg-47 polar contact is rarely populated during bMc b_5 MD simulations (*5*, *19*, *20*). The bMc b_5 crystal structure also shows that the solvent-exposed Ser-71 side chain is too small to make contact with those of Ile-25 and Phe-58, but that the Ser-71 β-CH_2 group does make van der Waals contact with heme and the aromatic side chain of Tyr-30.

Studies investigating the roles of motifs A and B in stabilizing OM b_5s relative to Mc b_5s have centered on "motif swap" mutants of rOM b_5. Complete replacement of motif A in rOM b_5 with the corresponding conserved Mc b_5 motif via the A18S/I32L/L47R triple mutant (hereafter rOM^{3M} b_5) led to modest decreases in holoprotein stability without significantly affecting apoprotein stability (*5*). The effects on holoprotein stability were magnified when motif B was subsequently swapped to give the A18S/I25L/I32L/L47R/L71S quintuple mutant (rOM^{5M} b_5) (*6*). In fact, rOM^{5M} b_5 is similar in stability to bMc b_5 at pH 7 with respect to several criteria, including midpoints of thermal and chemical denaturation. While a decrease in the strength of heme−polypeptide interactions may have played a role in this change, a factor of likely greater importance was the diminished thermodynamic stability of the corresponding apoprotein. The bulk of the apoprotein destabilization was traced to replacement of Leu-71 with Ser in the last turn of α5 in core 1 (*6*). On the basis of chemical denaturation data, we estimated that rOM^{L71S} and rOM^{5M} apo-b_5 are both at least ~2.4 kcal/mol less stable than rOM apo-b_5.

Available data suggest that thermodynamic stability and core 2 structure in Mc apo-b_5s are largely independent of core 1 properties. For example, mutations in core 1 of Mc b_5s can be rationally designed to either stabilize or destabilize the holo state without affecting the core 2 structure or stability in the apo state (*21*). Core 2 in rMc apo-b_5 has even been shown to fold natively when core 1 has been completely excised, albeit with some loss of thermodynamic stability (*22*). In contrast, the studies summarized above have shown that OM apo-b_5 stability involves a significant contribution from interactions involving Leu-71 in disordered core 1. The studies reported herein were undertaken with the goal of clarifying the greater role played by Leu-71 than of the entirety of motif A in stabilizing both the apo and holo forms of OM b_5s. A major driving force behind this effort is our hypothesis (*7*, *9*, *12*) that evolutionary divergence in Mc and OM b_5 stability is related to divergence in dynamic and redox properties, which were more likely important for adaptation to specialized subcellular roles (*4*, *23*, *24*).

Table 1: Results of Deconvolution[a] of Far-UV CD Data

	secondary structure content (%) (no. of residues)			
apoprotein	helix	strand	turn	unordered
rOM	17 (16)	22 (20)	15 (14)	45 (42)
rOM^{3M}	18 (17)	23 (21)	17 (16)	42 (39)
rOM^{L71S}	8 (7)	14 (13)	12 (11)	65 (60)

[a] Deconvolutions performed using CDSSTR (*28*, *29*).

MATERIALS AND METHODS

General. Generation, expression, and purification of the proteins employed in this study have been reported previously (*5*, *6*, *25*). Protein concentrations were determined on a Varian Carey 100 Bio UV−visible spectrometer, using the absorbance at 412 nm (Soret band λ_{max}) for the holoproteins, and at 280 nm for the apoproteins. For rOM holo-b_5 and bMc holo-b_5, an extinction coefficient of 130 000 M^{-1} cm^{-1} was used (*26*). Extinction coefficients at 280 nm for rOM apo-b_5 (ϵ = 12 950 M^{-1} cm^{-1}) and bMc apo-b_5 (ϵ = 11 460 M^{-1} cm^{-1}) were calculated on the basis of the number of Trp and Tyr residues in each protein (*27*).

Circular Dichroism Spectroscopy. CD spectra were recorded on a Jasco J-710 spectropolarimeter equipped with a Peltier thermostated cell holder. The temperature within the cell was monitored with an Omega model HH200 thermometer with a T thermocouple (±0.2 °C). Spectra were acquired at 1.0 nm intervals with a response time of 4 s and a scan rate of 50 nm/min, and represent the average of at least five scans. Background correction was accomplished by subtraction of a spectrum recorded at the same temperature and containing only buffer. Deconvolutions of far-UV CD spectra were performed using CDSSTR on the DICHROWEB web server (*28*, *29*).

Thermal Denaturation Studies. To test for isosbestic behavior during apoprotein unfolding, far-UV CD spectra were recorded at 6 °C intervals between 5 and 75 °C. Increments of 3 °C were used in the thermal denaturation experiments, for which the mean residue ellipticity at 222 nm (θ_{222}) over a 5 min period was recorded and averaged. An identical set of measurements was performed using a blank sample, and subtracted to correct for background changes. Samples were equilibrated for 15 min at each temperature prior to the recording of the data. Data were fit to the two-state equation noted in the text (*22*), kindly made available to us by J. Lecomte, using Igor Pro version 4.0 (Wavemetrics, Inc.). The mean values and average deviations from three independent runs are reported in Table 2.

Differential Scanning Calorimetry. Scanning calorimetry experiments were performed on a CSC 5100 Nano Differential Scanning Calorimeter (Calorimetry Sciences Corp., Provo, UT), using samples containing 1.9 mg/mL apoprotein that had been extensively dialyzed (four changes of buffer

Table 2: Denaturation Data

	CD				DSC			
	T_m (°C)	$\Delta H(T_m)$ (kcal/mol)	$\Delta S(T_m)$ (eu)	ΔG(25 °C) (kcal/mol)	ΔC_p (kcal mol^{-1} K^{-1})	ΔH_{cal} (kcal/mol)	ΔH_{vH} (kcal/mol)	$\Delta H_{cal}/\Delta H_{vH}$
rOM[a]	50.4 ± 0.4	36.3 ± 2.5	112 ± 8	1.8 ± 0.1	1.07 ± 0.04	35.7 ± 1.5	35.4 ± 1.6	1.01
rOM^{3M}	50.2 ± 0.3	35.6 ± 2.8	110 ± 9	1.8 ± 0.1	–	–	–	–
rOM^{L71S}	33.1 ± 0.3	26.3 ± 2.2	86 ± 7	0.5 ± 0.1	1.05 ± 0.05	27.2 ± 1.7	26.4 ± 1.8	1.03
bMc[a]	44.0 ± 0.4	43.2 ± 3.1	136 ± 10	2.0 ± 0.2	0.98 ± 0.04	42.9 ± 1.8	41.9 ± 1.7	1.02

[a] From ref *7*.

Table 3: Dynamic Light Scattering Data[a]

		folded			denatured (8 M urea)		
protein	T (°C)	R_H (nm)	P^b (%)	D^c ($\times 10^{-6}$ cm^2/s)	R_H (nm)	P^b (%)	D^c ($\times 10^{-7}$ cm^2/s)
rOM	5	1.85 ± 0.13	5.5 ± 0.2	0.73 ± 0.07	5.05 ± 0.23	14.1 ± 0.5	1.60 ± 0.11
rOM[d]	25	1.83 ± 0.13	5.3 ± 0.2	1.19 ± 0.09	5.52 ± 0.23	16.2 ± 0.6	3.83 ± 0.12
rOM^{3M}	25	1.81 ± 0.08	5.9 ± 0.4	1.21 ± 0.05	4.80 ± 0.18	13.6 ± 0.5	4.52 ± 0.08
rOM^{L71S}	5	3.03 ± 0.18	11.8 ± 0.4	0.44 ± 0.14	5.15 ± 0.26	19.6 ± 0.6	1.57 ± 0.12
bMc	5	2.02 ± 0.12	6.6 ± 0.3	0.66 ± 0.06	4.25 ± 0.18	12.1 ± 0.5	1.90 ± 0.13
bMc[d]	25	2.12 ± 0.13	7.1 ± 0.3	1.03 ± 0.06	4.64 ± 0.18	14.3 ± 0.6	4.70 ± 0.12

[a] Data recorded in 50 mM phosphate buffer (pH 7.0). [b] Polydispersity, a measure of the size distribution. [c] Diffusion coefficient. [d] From ref *7*.

every 6 h) against 50 mM potassium phosphate (pH 7.0). Immediately prior to each experiment, insolubles were removed by centrifugation at 12000*g* for 5 min and the sample was degassed at 0.5 atm for 15 min. Prior to the introduction of each sample, baselines were established via repeated scans in which the sample and reference cell contained buffer solution from the final dialysis step. Scans were performed from low to high temperatures ("upscans") at 1 K/min, followed by a downscan and a second upscan at the same rate to evaluate reversibility. Each experiment was repeated with a fresh apoprotein sample. Data from both upscans and the single downscan from each experiment were analyzed via a statistical mechanics-based deconvolution as implemented in the CSC 5100 software package to obtain the calorimetric enthalpy change (ΔH_{cal}), and via a nonlinear least-squares fit to a two-state model to obtain the van't Hoff enthalpy change (ΔH_{vH}). The mean values and average deviations from the six fits are reported in Table 2.

Dynamic Light Scattering. DLS measurements (*30*) were performed on a BI-200SM research goniometer and laser light scattering system, equipped with a BI-9000AT digital correlator (Brookhaven Instruments Corp.). Incident light with a λ of 532 nm (0.3−1.0 W) was used, with scattered light detected at an angle of 90° via a photomultiplier tube. The sample temperature was controlled by means of a thermostated cell jacket and monitored with the thermocouple described above. Samples (100 μM) were passed through 100 nm filters (Whatman) immediately before being used. All samples were buffered to pH 7 with 50 mM potassium phosphate. Experiments comparing bMc, rOM, and rOM^{L71S} apo-b_5 were performed at 5 °C, whereas experiments comparing bMc, rOM, and rOM^{3M} apo-b_5 were performed at 25 °C. Three independent measurements were performed for each protein, each consisting of six 30 s runs. The instrument software reports the results of each experiment as the average of the six runs. Data from one measurement on each protein are reported in Table 3 (the duplicate runs yielded essentially identical results). All data could be fitted multimodally, and essentially 100% of the scattering mass was attributed to a single low-molecular mass component. The diffusion coefficient (D) and the hydrodynamic radius (R_h) are related by the Stokes−Einstein equation (eq 1).

$$R_h = (kT)/(6\pi\eta D) \quad (1)$$

where T is the temperature in kelvin, k is the Boltzman constant (1.38×10^{-16} erg/K), and η is the solution viscosity. Values of η for urea solutions were determined by the method of Kawahara and Tanford (*31*).

RESULTS

Far-UV Circular Dichroism Studies. Far-UV circular dichroism (CD) spectra of rOM, rOM^{3M}, and rOM^{L71S} apo-b_5 recorded at 5 °C are compared in Figure 3A. Attempts were made to deconvolute these spectra to determine the distribution of residues in various secondary structure conformations. Most of the algorithms available for such deconvolutions (*28*, *29*) gave unreasonable or contradictory results, which we attribute to (1) the short and/or irregular nature of most of the α-helices and β-strands as shown in the holoprotein crystal structure and (2) the unusually large number of residues that exist in disordered conformations. The most realistic results (Table 1; see also Figure S1 of the Supporting Information) were obtained with CDSSTR, which iteratively removes proteins from the basis set used in fitting if they do not exhibit appropriate characteristics. The number of residues calculated by CDSSTR to exist in β-strand conformations in wild-type rOM apo-b_5 (20) is remarkably close to that expected on the assumption of similarity to rMc apo-b_5 as determined by NMR (*17*, *18*), namely, that $\beta1-\beta4$ (21 residues) retain holo-like secondary structure but that $\beta5$ (4 residues) is disordered. On the other hand, the calculated number of α-helical residues in rOM apo-b_5 (16) is higher than expected if we assume that α2−α5 of core 1 (∼24 helical residues in the holoprotein) are completely disordered, and that helicity is therefore entirely localized to α1 and α6 in core 2 (≤9 residues). This suggests the possibility that up to seven core 1 residues may be helical at any given time, which is not unrealistic given the observation by NMR of residual helicity in core 1 of rMc

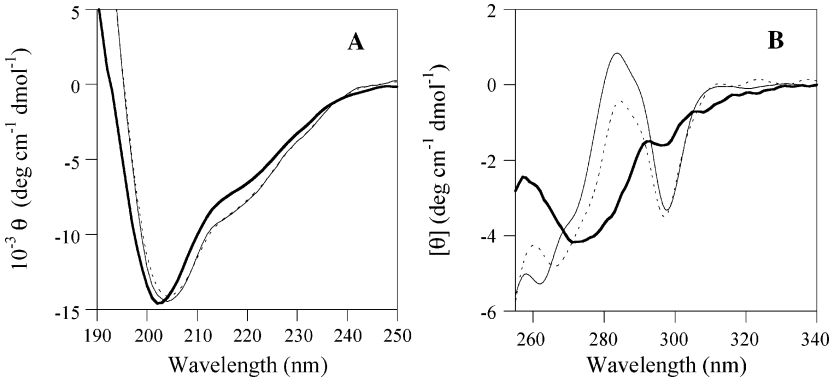

FIGURE 3: CD spectra of rOM apo-b_5 (thin solid line), rOM^{L71S} apo-b_5 (thick solid line), and rOM^{3M} apo-b_5 (dashed line) in the (A) far-UV region and (B) near-UV region. All data were recorded at 5 °C in 50 mM potassium phosphate buffer (pH 7.0).

apo-b_5 (*17*, *18*). Consistent with this possibility, the CDSSTR calculation for rOM apo-b_5 indicates that 42 residues are randomly configured. In contrast, we predicted a minimum of 50 disordered residues if core 1 is fully disordered (the polypeptide with the α2−α3−β5−α4−α5 organization contains ∼40 residues), because ∼10 residues near the protein N- and C-termini (italicized in Figure 1) are unstructured in rOM b_5 even when heme is present (*11*).

The far-UV CD spectra of rOM and rOM^{3M} apo-b_5 are virtually identical (Figure 3A and Table 1), demonstrating that the motif A swap has not significantly altered secondary structure content. In contrast, the far-UV CD spectrum of rOM^{L71S} apo-b_5 in Figure 3A exhibits diminished negative ellipticity in comparison to that of rOM apo-b_5 at wavelengths above 206 nm. The trough centered at 204 nm in the spectrum of rOM apo-b_5 is also shifted to 202 nm in rOM^{L71S} apo-b_5. Both changes suggest a modest decrease in the level of rOM^{L71S} apo-b_5 secondary structure, which the deconvolution data in Table 1 indicate is mainly due to a decrease in the number of residues in helices and β-strands. This suggests the intriguing possibility that the L71S mutation has caused conformational disorder in rOM apo-b_5 to extend beyond core 1 and into core 2. Other data (vide infra) argue against an alternate interpretation, namely, that the changes result from a substantial increase in the fraction of unfolded apoprotein in equilibrium with the folded form.

Near-UV CD Studies. Side chains of aromatic amino acids involved in well-defined tertiary packing interactions exhibit CD signals in overlapping regions of the near UV (Phe, 250−270 nm; Tyr, 270−290 nm; Trp, 280−300 nm) (*32*, *33*). On the basis of published studies with model peptides (*34*, *35*) and Mc apo-b_5s (*16*), the negative band at 298 nm in the spectrum of rOM apo-b_5 (Figure 3B) can be safely attributed to the Trp-22 side chain, which as already noted is located on the core 2 side of β4. The only two Phe residues in rOM b_5 are located near the center of core 1 helices (Phe−35 in α2 and Phe-58 in α4), which are largely disordered in the apo state, and are therefore unlikely to contribute significant dichroic activity in the near UV. The band centered at 262 nm with a shoulder near 272 nm in the rOM apo-b_5 near-UV CD spectrum is therefore likely dominated by contributions from tyrosine residues, all of which reside in the β-sheet (Tyr-6 and -7 in β1, Tyr-74 and -75 in β2, and Tyr-30 in β3). It is useful to point out that the side chains of three of these residues (Tyr-6, -7, and -75) contribute to core 2 tertiary structure in the rOM b_5 crystal structure.

The near-UV CD spectrum of rOM^{3M} apo-b_5 in Figure 3B exhibits relatively minor differences in comparison to that of wild-type rOM apo-b_5, indicating little effect on core 2 tertiary structure. This is consistent with the far-UV data which revealed no effect of the motif A swap on secondary structure. The near-UV CD spectrum of rOM^{L71S} apo-b_5, in contrast, differs markedly from that of wild-type rOM apo-b_5. The magnitudes of the changes are inconsistent with a conclusion that the L71S mutation has resulted in an increase in the level of the unfolded apoprotein in equilibrium with the folded form. The region near 300 nm in the rOM^{L71S} apo-b_5 spectrum is nearly featureless, suggesting almost complete loss of tertiary structure in core 2 near the Trp-22 side chain in β4 and/or greatly increased mobility of that side chain. The other changes in the spectrum are indicative of a change in environment or an increase in mobility of some or all of the Tyr side chains in β1−β3. The combined far-UV and near-UV CD data therefore strongly suggest that the L71S mutation has led to substantial disruption of core 2 tertiary structure in the folded form of rOM apo-b_5, due in significant measure to partial loss of secondary structure of β1−β4.

Thermal Denaturation Studies. We recently reported results of thermal denaturation studies monitored by CD spectroscopy and by differential scanning calorimetry (DSC), which revealed that rOM and bMc apo-b_5 exhibit reversible, two-state unfolding at pH 7 (*7*). Thermodynamic data obtained in those studies are compiled in Table 2. To obtain additional insight into relative effects of the L71S mutation and the motif A swap on the unfolding thermodynamics rOM apo-b_5, we performed thermal denaturation studies of rOM^{3M} and rOM^{L71S} apo-b_5 monitored by CD spectroscopy. For rOM^{L71S} apo-b_5, we also examined thermal denaturation by DSC.

CD spectra of rOM^{3M} and rOM^{L71S} apo-b_5 recorded prior to thermal denaturation and after each denatured protein had been returned to the initial conditions exhibited no significant differences, indicating that the mutations have not affected the reversibility of thermal denaturation. In addition, CD spectra of the two mutants recorded as a function of increasing temperature exhibit isodichroic points, consistent with two-state behavior. Thermal denaturation curves for rOM^{3M} and rOM^{L71S} apo-b_5 obtained in experiments in which the time-averaged value of ellipticity at 220 nm was recorded are compared in Figure 4. The rOM^{3M} apo-b_5 denaturation curve is virtually identical to that previously reported for

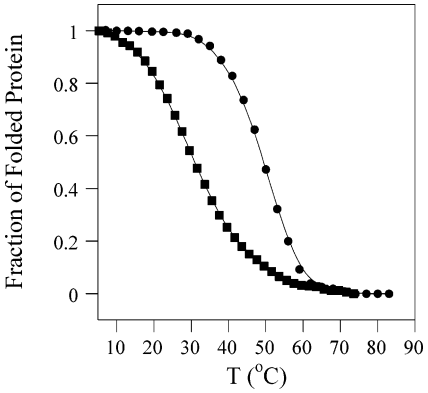

FIGURE 4: Data from thermal denaturation experiments monitored by CD spectroscopy for rOM^{3M} apo-b_5 (●) and rOM^{L71S} apo-b_5 (■). Both samples were buffered to pH 7.0 with 50 mM phosphate. Solid lines through the data points represent fits of the data to an equation describing a two-state unfolding process.

wild-type rOM apo-b_5, exhibiting well-defined plateaus in the native and unfolded regions. The corresponding curve for rOM^{L71S} apo-b_5 is displaced toward lower temperatures, and exhibits a shorter and less well-defined plateau in the native region. The presence of even such a short plateau nevertheless provides additional evidence that little rOM^{L71S} apo-b_5 exists in the unfolded state at temperatures near 5 °C.

As observed for wild-type rOM apo-b_5, the thermal denaturation curves for rOM^{3M} and rOM^{L71S} apo-b_5 were fit well by a two-state model. The model we used (*22*) combines linear equations relating the fraction of protein in the folded and unfolded state at each temperature with an expanded form of the Gibbs−Helmholtz equation (eq 2), and accounts for non-zero slopes in the native and denaturing regions.

$$\Delta G(T) = \Delta S(T_m)(T_m - T) - \Delta C_p(T_m - T) + T\Delta C_p \ln(T_m/T) \quad (2)$$

$$\Delta S(T_m) = \Delta H(T_m)/T_m \quad (3)$$

The model provides the thermal denaturation midpoint (T_m value), the unfolding entropy referenced to the T_m [$\Delta S(T_m)$], and the associated heat capacity change (ΔC_p), but more accurate results can be obtained if ΔC_p is introduced as a constant. In fitting of the data for rOM^{L71S} apo-b_5, we used the ΔC_p value obtained in the DSC studies described below (Table 2), which is virtually identical to that previously reported for wild-type rOM apo-b_5 (*7*). This surprising observation encouraged us to use the ΔC_p value for wild-type rOM apo-b_5 in fitting of the CD denaturation curve for rOM^{3M} apo-b_5. Unfolding enthalpies referenced to the T_m for rOM^{3M} and rOM^{L71S} apo-b_5 shown in Table 2 were obtained using eq 3.

A calorimetric scan for rOM^{L71S} apo-b_5 is compared with a previously reported scan for wild-type rOM apo-b_5 (*7*) in Figure 5. The data show that rOM^{L71S} apo-b_5 behaves like rOM and bMc apo-b_5 in exhibiting a single reversible transition that is fit well by a two-state model. The unfolding enthalpy referenced to the T_m obtained in this manner is called the van't Hoff enthalpy (ΔH_{vH}, Table 2). The DSC data for rOM^{L71S} apo-b_5 were also subjected to a statistical mechanics-based deconvolution to obtain the overall (model-independent) enthalpy change (calorimetric enthalpy, ΔH_{cal}) (Table 2). As previously demonstrated for rOM and bMc apo-b_5, ΔH_{cal} and ΔH_{vH} for rOM^{L71S} apo-b_5 differ by less than 3%, providing the most convincing evidence that the rOM^{L71S} apo-b_5 unfolding reaction obeys a two-state equilibrium (*36*). It is also noteworthy that thermal denaturation data for rOM^{L71S} apo-b_5 obtained by CD and by DSC are virtually identical despite the use of very different apoprotein concentrations (15 and 185 μM, respectively), strongly suggesting little if any tendency toward self-association.

The thermal denaturation data show that the motif A swap exerted virtually no effect on rOM apo-b_5 unfolding thermodynamics, consistent with the previously reported chemical denaturation studies (*6*). Also consistent with those studies, we observed that the L71S mutation compromised rOM apo-b_5 thermodynamic stability as highlighted by a 17 °C decrease in T_m. Using the T_m, $\Delta H(T_m)$, and ΔC_p values for the b_5 variants shown in Table 2, we calculated approximate unfolding free energies ($\Delta G_{N\rightarrow U}$ values) at 25 °C via eq 2. The $\Delta G_{N\rightarrow U}$ values obtained in this manner for rOM, rOM^{3M}, and bMc apo-b_5 at 25 °C are virtually identical, consistent with our previously reported GdmCl-mediated denaturation studies (*5*). The $\Delta G_{N\rightarrow U}$ values in Table 2 indicate that the L71S mutation has destabilized rOM apo-b_5 by 1.3 kcal/mol at 25 °C, significantly less than the 2.4 kcal/mol destabilization estimated from GdmCl denaturation data (*6*). The fraction of rOM^{L71S} apo-b_5 that exists in the folded state at 25 °C as determined in the heat-mediated denaturation studies reported herein (70%) and that in the

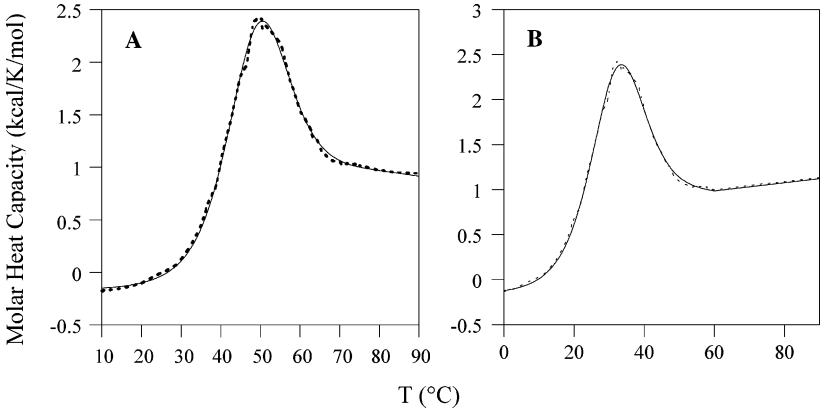

FIGURE 5: DSC data for (A) rOM apo-b_5 (1.87 mg/mL) (*7*) and (B) rOM^{L71S} apo-b_5 (1.94 mg/mL). The dashed line in each panel indicates the observed data, and the solid line is the fit of the data to an equation representing a two-state transition. All samples were buffered to pH 7.0 with 50 mM phosphate buffer.

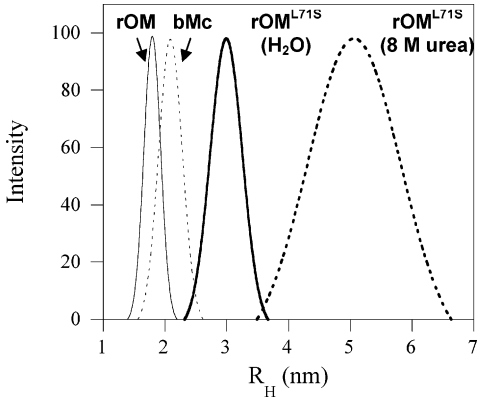

FIGURE 6: Size distribution plots of DLS data obtained for rOM apo-b_5 (thin solid line), bMc apo-b_5 (thin dashed line), and rOM^{L71S} apo-b_5 (thick solid line) in aqueous solution, and for rOM^{L71S} apo-b_5 in the presence of 8 M urea (thick dashed line). These experiments were performed at 5 °C and pH 7 (50 mM potassium phosphate).

previously reported GdmCl-mediated unfolding studies (80%) are strikingly similar, however.

Dynamic Light Scattering. To further examine the consequences of the motif A swap and the L71S mutation on rOM apo-b_5 properties, we performed dynamic light scattering (DLS) experiments at pH 7 in aqueous solution (native conditions) and in the presence of 8 M urea (denaturing conditions). DLS experiments comparing rOM, rOM^{L71S}, and bMc apo-b_5 were performed at 5 °C to minimize the fraction of rOM^{L71S} apo-b_5 that is present in the unfolded state in aqueous solution. The corresponding experiments comparing rOM, rOM^{3M}, and bMc apo-b_5 were performed at 25 °C. Hydrodynamic radii (R_H), polydispersity values, and diffusion constants obtained in all of the DLS experiments are compiled in Table 3. Size distribution plots of the DLS data for rOM, rOM^{L71S}, and bMc apo-b_5 in aqueous solution, and for rOM^{L71S} apo-b_5 in 8 M urea, are compared in Figure 6.

The data reveal that R_H and polydispersity values for the folded apoproteins increase in the following order: rOM apo-b_5 ~ rOM^{3M} apo-b_5 < bMc apo-b_5 < rOM^{L71S} apo-b_5. Thus, only the L71S mutation caused a significant increase in the size and size distribution of rOM apo-b_5, but the effect is much larger than anticipated on the basis of our previous studies comparing bMc and rOM apo-b_5. In fact, Figure 6 shows the absence of significant overlap of the rOM^{L71S} apo-b_5 size distribution plot with that of rOM apo-b_5, and only minor overlap with that of bMc apo-b_5. The size distribution plot for rOM^{L71S} apo-b_5 in aqueous solution (Figure 6) is highly symmetrical and exhibits only minor overlap with the corresponding plot for the urea-denatured state, further evidence that little if any rOM^{L71S} apo-b_5 is present in the unfolded state at 5 °C. In addition, rOM^{L71S} apo-b_5 DLS parameters obtained using protein concentrations of 15 and 100 μM are virtually identical, supporting the thermal denaturation data in indicating little if any tendency toward self-association. These observations provide further strong evidence that the L71S mutation in rOM b_5 not only has led to an increase in the extent to which core 1 expands upon loss of heme but also has caused conformational disruption to extend into core 2 leading to additional expansion.

Chemical Cross-Linking. As part of our investigation into the effects of the L71S mutation on rOM apo-b_5 properties, we treated rOM and rOM^{L71S} apo-b_5 (40 μM) with the cross-linking agent 1-ethyl-3-[3-(dimethylamino)propyl]carbodiimide hydrochloride (EDC, 100 μM) for 2 h at 4 °C and pH 7. We have already reported that wild-type rOM apo-b_5 is not susceptible to EDC-mediated cross-linking at 25 °C (*7*), and we find no evidence that it undergoes significant cross-linking at 4 °C either. In contrast, SDS−PAGE analysis of the reaction between EDC and rOM^{L71S} apo-b_5 at 4 °C (not shown) revealed weak but distinct bands of ~22 and ~33 kDa, in addition to the much stronger band at 11 kDa arising from the monomer.

As already noted, the absence of concentration dependence in DLS and thermal denaturation studies of rOM^{L71S} apo-b_5 strongly suggests that the mutant apoprotein is almost exclusively monomeric at concentrations up to 180 μM. Nonetheless, the chemical cross-linking studies clearly demonstrate that rOM^{L71S} apo-b_5 is more prone to self-associate than wild-type rOM apo-b_5 at 4 °C, a temperature at which our data indicate that both apoproteins are fully folded. Because self-association is typically driven by hydrophobic interactions, this observation suggests that the expansion of core 1 and the partial unfolding of core 2 of rOM apo-b_5 caused by the L71S mutation resulted in an increase in the solvent-exposed hydrophobic surface area.

Core 1 Hydropathicity Calculations. We have suggested that the greater compactness of core 1 in rOM apo-b_5 in comparison to bMc apo-b_5 is a consequence of greater hydrophobicity arising from motifs A and B (*7*). It was therefore of interest to compare the impact of the motif A swap and of the L71S mutation on core 1 hydrophobicity. For this purpose, we consider core 1 to comprise residues 33−72 (defining α2−α3−β5−α4−α5 and associated core 1 loops) and residues 18, 23, 25, 30, and 32 (all within or directly abutting the β-sheet in core 2 with side chains facing core 1). The overall polarity of core 1 in rOM and bMc apo-b_5 was assessed via the Grand Average of Hydropathicity (GRAVY) method of Kyte and Doolittle (*37*), which involves summing the hydropathicity values of the component residues (<0 for polar residues; >0 for nonpolar residues) and dividing by the total number of residues (in this case, 44). The core 1 GRAVY score of rOM apo-b_5 (−0.371) is less negative than that of bMc b_5 (−0.798), highlighting its overall lower polarity. rOM^{5M} b_5, in which motifs A and B have both been swapped for the corresponding Mc b_5 residues, has a core 1 GRAVY score of −0.731, similar to that of bMc b_5. It is noteworthy, however, that the motif A swap causes a larger decrease in the rOM b_5 core 1 GRAVY score (to −0.629) than does replacement of Leu-71 in rOM b_5 motif B with Ser (to −0.473). Hence, the larger role played by Leu-71 than by motif A in rOM apo-b_5 properties cannot be explained by a larger contribution to core 1 hydrophobicity. Neither, therefore, can the greater compactness of core 1 of rOM apo-b_5 in comparison to that of bMc apo-b_5 be entirely explained by a higher overall hydrophobicity.

DISCUSSION

Insight into the Relationship between Apoprotein Properties and Holoprotein Stability in b_5s. In a recent study investigating the relationship between heme binding and stability in rMc b_5 (*21*), Mukhopadhyay and Lecomte compared the effect of mutations within the heme-binding loop (core 1) and in the heme-independent folding core (core

2). All mutations involved surface-exposed residues located distant from the core 1−core 2 interface. They reported one core 2 mutation involving a residue in α6, which decreased holoprotein stability by lowering apoprotein thermodynamic stability. Effects of this type of mutation on holoprotein stability can be understood, in simple terms, by the fact that it requires an increased fraction of heme binding energy to be invested in maintaining the native holoprotein structure. Two mutations in core 1 of rMc b_5 were reported, one designed to stabilize α4 and the other to destabilize the same helix. Both mutations exerted the anticipated effects on holoprotein stability without significantly altering apoprotein thermodynamic stability and structure (*21*). This can be understood in terms of the induced-fit model of protein/cofactor recognition by the fact that little if any nativelike structure exists in core 1 of the wild-type or mutant Mc apo-b_5s. Thus, the mutations in α4 neither enhance nor diminish the extent to which core 1 becomes structured upon heme binding.

Our studies have indicated that the greater stability exhibited by OM holo-b_5s in comparison to Mc holo-b_5s does have a large contribution from a smaller conformational change associated with heme binding, but not due to the presence of greater holo-like structure or a smaller number of conformationally disordered residues in the apo state (*7*). We have instead argued that it is primarily a consequence of more extensive residual hydrophobic interactions in OM apo-b_5s, which reduces the number of non-native conformations that can be explored by core 1 in comparison to Mc apo-b_5s and is manifested in a more compact empty heme-binding pocket.

The motif A swap in rOM b_5 involved one residue in a core 1 helix that is distant from the interface in α4 (Leu-47) and one in a flexible surface-exposed loop between two β-sheet strands (Ala-18). The third residue (Ile-32) is located precisely at the core 1−core 2 juncture, between the C-terminus of β3 and the N-terminus of α2. It can therefore be assumed that none of the residues involved in the motif A swap participate in stable units of secondary or tertiary structure in rOM apo-b_5, and our far-UV and near-UV CD studies have shown that the motif A swap does not introduce or disrupt structure. Given the results summarized above for rMc b_5 mutations, the observation that the motif A swap modestly decreases rOM holo-b_5 stability without affecting apoprotein stability is not surprising. [The holoprotein destabilization likely arises because replacing Ile-32 with Leu affects heme−polypeptide interactions (*5*).] Our DLS data further revealed that the motif A swap caused little if any change in rOM apo-b_5 size (R_H) or size distribution (polydispersity). While this is consistent with our hypothesis that core 1 compactness in the apo-b_5 state plays a key role in tuning holoprotein stability, it is puzzling given the large decrease in core 1 hydrophobicity associated with the motif A swap.

In contrast to the motif A swap, the L71S mutation caused a large increase in rOM apo-b_5 R_H and polydispersity values. If our hypothesis regarding binding pocket compactness and holoprotein stability is correct, this suggests that the decrease in rOM holo-b_5 stability caused by the L71S mutation has a significant entropic component due to an increase in the number of conformations that are populated by the disordered region of rOM apo-b_5. In any event, it allows a firm conclusion that Leu-71 plays a much larger role than the entirety of motif A in rendering core 1 in OM apo-b_5s more compact and less dynamic than core 1 in Mc apo-b_5s.

As already demonstrated previously (*6*), the L71S mutation also differed from the motif A swap in causing a significant decrease in rOM apo-b_5 stability. The thermal denaturation data reported herein reveal that this is due in part to a less positive enthalpy of unfolding, suggesting weakened bonding interactions in the folded state. There is also a contribution from a less positive unfolding entropy, possibly reflecting a smaller overall increase in the level of polypeptide conformational disorder upon unfolding. Both interpretations are supported by the observation that the L71S mutation disrupted secondary and tertiary structure in core 2, thereby increasing the number of amino acids that are disordered in the apo state. Also consistent with this interpretation is our observation in DLS studies that rOM^{L71S} apo-b_5 is considerably larger and more polydisperse than bMc apo-b_5. What makes the effects of the L71S mutation on core 2 structure and rOM apo-b_5 stability most intriguing is the fact that Leu-71 resides in disordered core 1.

The roles played by Leu-71 of motif B in OM apo-b_5s in defining tertiary structure in core 2, maintaining disordered core 1 in a compact state, and providing overall thermodynamic stability to the partially folded apoprotein are clearly inter-related. The greater hydrophobicity of Leu-71 in OM apo-b_5s in comparison to that of Ser-71 in Mc apo-b_5s is certainly important in this respect. This begs the question, then, of why residues contributing to motif A do not play an equally important role. The backbones of four residues involved in the conserved rOM b_5 packing motif described above either are in (Ile-25 and Met-23 in β4 and Tyr-30 in β3) or directly abut (Ile-32) the β-sheet with their side chains formally in core 1, as are the corresponding residues in bMc b_5 (Leu-25, Leu-23, Tyr-30, and Leu-32). Available evidence indicates that the β-sheet in Mc (*17*, *18*) and OM b_5 (*7*) remains intact in the apo state, limiting backbone mobility of residues 23, 25, 30, and 32, but the absence of tertiary structure in core 1 can be expected to increase the conformational flexibility of their side chains. The van der Waals contacts involving those side chains observed in the rOM and bMc b_5 crystal structures are therefore likely to persist in the corresponding apoproteins, albeit in a less specific and more dynamic assembly. The solution NMR structure of rMc apo-b_5 supports this idea, and suggests that other nonnative hydrophobic contacts involving side chains of hydrophobic core 1 residues may also be explored (*17*, *18*).

We propose that the relatively immobile hydrophobic side chains on the core 1 side of the β-sheet serve to template a general hydrophobic collapse of core 1 in both Mc and OM apo-b_5s, which is more extensive in the latter primarily because Leu occupies position 71 rather than Ser. We attribute the larger role played by Leu-71 than by motif A in the more extensive rOM apo-b_5 core 1 collapse to its proximity to the juncture between disordered core 1 and core 2, which entropically favors residual interactions with hydrophobic side chains on the core 1 side of the β-sheet. The only core 1 residue in OM b_5 motif A having a side chain much more hydrophobic (Leu-47) than its Mc counterpart (Arg-47) is located comparatively distant from the core 1−core 2 junctures, and is therefore less predisposed to engage in such residual hydrophobic interactions.

We propose that participation of Leu-71 in a general hydrophobic collapse of core 1 in rOM apo-b_5 has the reciprocal effect of stabilizing the β-sheet by minimizing backbone dynamic mobility, and that this has the added consequence of stabilizing tertiary structure involving the side chains of Trp-22 and other residues with backbones in the β-sheet and side chains on the core 2 side. The fact that core 2 secondary and tertiary structure in Mc apo-b_5s is not similarly dependent on a residue with a bulky hydrophobic side chain at position 71 provides fresh evidence (*6*, *7*) for evolution of compensating structural factors elsewhere in their structures.

Possible Relevance to Function. The large stability difference exhibited by OM and Mc b_5s may not by itself be important with respect to the specialized roles played by the two isoforms. Rather, we have proposed (*7*, *9*, *12*) that it is either a source or a consequence of other divergent biophysical properties that are functionally important. As already noted, the greater stability of OM b_5s relative to that of Mc b_5s appears to be due in part to lower core 1 polypeptide dynamic mobility (*5*, *9*, *19*). Evolutionary divergence of polypeptide dynamic mobility in the vicinity of heme may have played a key role in adapting Mc and OM b_5s for interactions with electron transfer partners that differ not only in identity but perhaps also in number. We have also considered the possibility that nature has employed divergence in Mc and OM b_5 stability as a means of differentiating their reduction potentials (*7*, *9*, *12*), which has occurred with little or no change in factors most commonly associated with such a phenomenon (ligation, electrostatic environment, and solvent exposure of heme). Indeed, studies with bishistidine-ligated heme protein models have revealed that increases in the level of hydrophobic packing interactions that decrease peptide dynamic mobility (*38*) stabilize His−Fe(III) coordination to a greater extent than His−Fe(II) coordination and thereby lead to a negative shift in reduction potential (*39*). Both of these possible functional roles for evolutionary divergence in OM and Mc b_5 stability suggest that a path involving changes within the heme-binding pocket region (core 1) may have been more advantageous than one involving a change in overall apoprotein stability. Such a path may also have been driven by another factor, namely, the need to maintain adequate levels of the holo form of each isoform. We have shown that complete replacement of motifs A and B in rOM b_5 greatly slowed holoprotein production in our *Escherichia coli* expression system due to severely compromised apoprotein longevity (*7*). We observed similar effects due to the L71S mutation in this study.

A search of available databases has shown that residue 71 is either Leu or Met in all known b_5s from insects, plants, and fungi (*40*). It can therefore be concluded that one of those hydrophobic residues occupied position 71 in the common precursor of mammalian Mc and OM b_5, but was replaced by the much more polar Ser in the eventual Mc isoform. We propose that this change was of prime importance in allowing stability properties of the two isoforms to diverge, along with related properties of more likely benefit with respect to function. This report shows that the L71S mutation in OM b_5 as it exists today also compromises holoprotein stability, but with major contributions from thermodynamic destabilization of the apoprotein and an increase in the number of residues that are disordered in the apo state. Efforts aimed at identifying additional conserved differences in packing interactions in Mc and OM b_5s that limit differences in conformational disorder to core 1 of the former while allowing Ser to occupy position 71 will be reported in due course.

ACKNOWLEDGMENT

We thank Prof. Russell Middaugh for use of his DLS and DSC equipment.

SUPPORTING INFORMATION AVAILABLE

Results of fitting of far-UV CD spectra using CDSSTR. This material is available free of charge via the Internet at http://pubs.acs.org.

REFERENCES

1. Lederer, F., Ghrir, R., Guiard, B., Cortial, S., and Ito, A. (1983) Two Homologous Cytochromes b_5 in a Single Cell, *Eur. J. Biochem. 132*, 95−102.
2. Kuroda, R., Ikenoue, T., Honsho, M., Tsujimoto, S., Mitoma, J., and Ito, A. (1998) Charged amino acids at the carboxy-terminal portions determine the intracellular locations of two isoforms of cytochrome b_5, *J. Biol. Chem. 273*, 31097−31102.
3. Ozols, J. (1989) Structure of cytochrome b_5 and its topology in the microsomal membrane, *Biochim. Biophys. Acta 997*, 121−130.
4. Vergeres, G., and Waskell, L. (1995) Cytochrome b_5, its functions, structure and membrane topology, *Biochimie 77*, 604−620.
5. Altuve, A., Silchenko, S., Lee, K.-H., Kuczera, K., Terzyan, S., Zhang, X., Benson, D. R., and Rivera, M. (2001) Probing the differences between rat liver outer mitochondrial membrane cytochrome b_5 and microsomal cytochromes b_5, *Biochemistry 40*, 9469−9483.
6. Cowley, A. B., Altuve, A., Kuchment, O., Terzyan, S., Zhang, X., Rivera, M., and Benson, D. R. (2002) Toward engineering the stability and hemin binding properties of microsomal cytochromes b_5 into rat outer mitochondrial membrane cytochrome b_5: Examining the influence of residues 25 and 71, *Biochemistry 41*, 11566−11581.
7. Cowley, A. B., Rivera, M., and Benson, D. R. (2004) Stabilizing roles of residual structure in the empty heme binding pockets and unfolded states of microsomal and mitochondrial apocytochrome b_5, *Protein Sci. 13*, 2316−2329.
8. Silchenko, S., Sippel, M. L., Kuchment, O., Benson, D. R., Mauk, A. G., Altuve, A., and Rivera, M. (2000) Hemin is kinetically trapped in cytochrome b_5 from rat outer mitochondrial membrane, *Biochem. Biophys. Res. Commun. 271*, 467−472.
9. Simeonov, M., Altuve, A., Massiah, M. A., Wang, A., Eastman, M. A., Benson, D. R., and Rivera, M. (2005) Mitochondrial and Microsomal Ferric b_5 Cytochromes Exhibit Divergent Conformational Plasticity in the Context of a Common Fold, *Biochemistry 44*, 9308−9319.
10. Durley, R. C. E., and Mathews, F. S. (1996) Refinement and Structural Analysis of Bovine Cytochrome b_5 at 1.5 Å Resolution, *Acta Crystallogr. D52*, 65−76.
11. Rodriguez-Maranon, M. J., Qiu, F., Stark, R. E., White, S. P., Zhang, X., Foundling, S. I., Rodriguez, V., Schilling, C. L., III, Bunce, R. A., and Rivera, M. (1996) ^{13}C NMR spectroscopic and X-ray crystallographic study of the role played by mitochondrial cytochrome b_5 heme propionates in the electrostatic binding to cytochrome *c*, *Biochemistry 35*, 16378−16390.
12. Altuve, A., Wang, L., Benson, D. R., and Rivera, M. (2004) Mammalian mitochondrial and microsomal cytochromes b_5 exhibit divergent structural and biophysical characteristics, *Biochem. Biophys. Res. Commun. 314*, 602−609.
13. Storch, E. M., and Daggett, V. (1996) Structural Consequences of Heme Removal: Molecular Dynamics Simulations of Rat and Bovine Apocytochrome b_5, *Biochemistry 35*, 11596−11604.
14. Cheng, Q., Sun, N., Rivera, M., Benson, D. R., and Kuczera, K. Manuscript in preparation.
15. Banci, L., Bertini, I., Rosato, A., and Scacchieri, S. (2000) Solution Structure of Oxidized Microsomal Rabbit Cytochrome b_5, *Eur. J. Biochem. 267*, 755−766.

16. Huntley, T. E., and Strittmatter, P. (1972) The effect of heme binding on the tryptophan residue and the protein conformation of cytochrome b_5, *J. Biol. Chem. 247*, 4641−4647.
17. Falzone, C. J., Mayer, M. R., Whiteman, E. L., Moore, C. D., and Lecomte, J. T. J. (1996) Design Challenges for Hemoproteins: The Solution Structure of Apocytochrome b_5, *Biochemistry 35*, 6519−6526.
18. Falzone, C. J., Wang, Y., Vu, B. C., Scott, N. L., Bhattacharya, S., and Lecomte, J. T. J. (2001) Structural and dynamic perturbations induced by heme binding in cytochrome b_5, *Biochemistry 40*, 4879−4891.
19. Lee, K.-H., and Kuczera, K. (2003) Molecular Dynamics Simulation Studies of Cytochrome b_5 from Outer Mitochondrial and Microsomal Membrane, *Biopolymers 69*, 260−269.
20. Storch, E. M., and Daggett, V. (1995) Molecular Dynamics Simulation of Cytochrome b_5: Implications for protein−protein recognition, *Biochemistry 34*, 9682.
21. Mukhopadhyay, K., and Lecomte, J. T. J. (2004) A Relationship between Heme Binding and Protein Stability in Cytochrome b_5, *Biochemistry 43*, 12227−12236.
22. Constans, A. J., Mayer, M. R., Sukits, S. F., and Lecomte, J. T. J. (1998) A test of the relationship between sequence and structure in proteins: Excision of the heme binding site in apocytochrome b_5, *Protein Sci. 7*, 1983−1993.
23. Ogishima, T., Kinoshita, J.-y., Mitani, F., Suematsu, M., and Ito, A. (2003) Identification of Outer Mitochondrial Membrane Cytochrome b_5 as a Modulator for Androgen Synthesis in Leydig Cells, *J. Biol. Chem. 278*, 21204−21211.
24. Soucy, P., and Luu-The, V. (2002) Assessment of the ability of type 2 cytochrome b_5 to modulate 17,20-lyase activity of human P450c17, *J. Steroid Biochem. Mol. Biol. 80*, 71−75.
25. Rivera, M., Barillas-Mury, C., Christensen, K. A., Little, J. W., Wells, M. A., and Walker, F. A. (1992) Gene synthesis, bacterial expression, and ^{1}H NMR spectroscopic studies of the rat outer mitochondrial membrane cytochrome b_5, *Biochemistry 31*, 12233−12240.
26. Beck von Bodman, S., Schuler, M. A., Jollie, D. R., and Sligar, S. G. (1986) Synthesis, bacterial expression, and mutagenesis of the gene coding for mammalian cytochrome b_5, *Proc. Natl. Acad. Sci. U.S.A. 83*, 9443−9447.
27. Gill, S. C., and von Hippel, P. H. (1989) Calculation of protein extinction coefficients from amino acid sequence data, *Anal. Biochem. 182*, 319−326.
28. Lobley, A., Whitmore, L., and Wallace, B. A. (2002) DICHROWEB: An interactive website for the analysis of protein secondary structure from circular dichroism spectra, *Bioinformatics 18*, 211−212.
29. Whitmore, L., and Wallace, B. A. (2004) DICHROWEB, an online server for protein secondary structure analyses from circular dichroism spectroscopic data, *Nucleic Acids Res. 32*, W668−W673.
30. Schmitz, K. S. (1990) *An introduction to dynamic light scattering by macromolecules*, Academic Press, Boston.
31. Kawahara, K., and Tanford, C. (1966) Viscosity and density of aqueous solutions of urea and guanidinium hydrochloride, *J. Biol. Chem. 241*, 3228−3232.
32. Kahn, P. C. (1979) The interpretation of near-ultraviolet circular dichroism, *Methods Enzymol. 61*, 339−378.
33. Strickland, E. H. (1974) Aromatic contributions to circular dichroism spectra of proteins, *Crit. Rev. Biochem. 2*, 113−174.
34. Strickland, E. H., Horwitz, J., and Billups, C. (1969) Fine Structure in the Near-Ultraviolet Circular Dichroism and Absorption Spectra of Tryptophan Derivatives and Chymotrypsinogen A at 77 K, *Biochemistry 8*, 3205−3213.
35. Edelhoch, H., Lippoldt, R. E., and Wilchek, M. (1968) The Circular Dichroism of Tyrosyl and Tryptophanyl Diketopiperazines, *J. Biol. Chem. 243*, 4799−4805.
36. Zhou, Y., Hall, C. K., and Karplus, M. (1999) The calorimetric criterion for a two-state process revisited, *Protein Sci. 8*, 1064−1074.
37. Kyte, J., and Doolittle, R. F. (1982) A simple method for displaying the hydropathic character of a protein, *J. Mol. Biol. 157*, 105−132.
38. Liu, D., Williamson, D. A., Kennedy, M. L., Williams, T. D., Morton, M. M., and Benson, D. R. (1999) Aromatic Side Chain-Porphyrin Interactions in Designed Hemoproteins, *J. Am. Chem. Soc. 121*, 11798−11812.
39. Kennedy, M. L., Silchenko, S., Houndonougbo, N., Gibney, B. R., Dutton, P. L., Rodgers, K. R., and Benson, D. R. (2001) Model Hemoprotein Reduction Potentials: The Effects of Histidine to Iron Coordination Equilibrium, *J. Am. Chem. Soc. 123*, 4635−4636.
40. Wang, L., Terzyan, S., Zhang, X., and Benson, D. R. Manuscript in preparation.
41. Mathews, F. S., Gerwinsky, E. W., and Argos, P. (1979) The X-ray Crystallographic Structure of Calf Liver Cytochrome b_5, in *The Porphyrins* (Dolphin, D., Ed.) pp 107−147, Academic Press, New York.

BI051337M